Cement and Concrete Research 39 (2009) 1087–1094

Contents lists available at ScienceDirect

Cement and Concrete Research

journal homepage: http://ees.elsevier.com/CEMCON/default.asp

Mechanical and fracture properties of cement-based bi-materials after thermal cycling

Antonios Kanellopoulos [a,*], Farhat A. Farhat [b], Demetrios Nicolaides [c], Bhushan L. Karihaloo [d]

[a] School of Engineering, University of Cyprus, 75 Kallipoleos Avenue, P.O. Box 20537, 1678, Nicosia, Cyprus
[b] Higher Institute of Engineering, Hoon, Libya
[c] School of Engineering, Frederick Institute of Technology, Nicosia, Cyprus
[d] School of Engineering, Cardiff University, Cardiff, CF24 3AA, UK

ARTICLE INFO

Article history:
Received 16 June 2008
Accepted 14 July 2009

Keywords:
High-performance concrete (E)
Bi-materials (D)
Fracture properties (C)
Thermal treatment (A)
Mechanical properties (C)

ABSTRACT

This study investigates the effect of thermal cycles on the fracture properties of the cement-based bi-materials. Sixty eight cubes were exposed to a varied number of 24-hour thermal cycles ranging from 0 to 90 and subsequently were tested in a wedge splitting configuration. The mechanical and fracture properties of normal strength and high strength concretes are substantially improved after 30 thermal cycles, but less so after 90 thermal cycles both in isolation and when bonded to an ultra high-performance fibre-reinforced cement-based composite.

1. Introduction

The mechanical behaviour of structures is greatly influenced by the materials used in their construction. Based on their tensile stress–deformation response, most engineering materials can be categorized into; brittle, ductile and quasi-brittle. Plain and reinforced concrete belong to the last category. Structures made of concrete contain inherent flaws, such as water filled pores, air voids, shrinkage cracks, even prior to the application of load. These flaws, and especially the small cracks (micro-cracks), grow stably under external loading and coalesce with existing or newly-formed micro-cracks until large fractures are formed which cause the collapse of the structure. To date structures are designed without regard to either the propagation of large cracking zones through them or an energy failure criterion. Fracture mechanics provides an energy based failure theory that could be used in designing cement-based structures against the consequences of crack initiation and propagation [1].

Much attention has been paid to the mechanical and fracture properties of concrete at room temperature, including strength, stiffness, toughness and brittleness. Information about these properties under high temperature environment, however, is very useful for designing concrete structures subject to various high temperature environments. So far, much attention has been paid to the study of concrete strength and stiffness [2–5] under various heating scenarios (heating rate, maximum heating temperature, exposure period, heat cycle). Some work has also been done on concrete toughness [6], and brittleness and fracture energy [7–9]. Most of these studies have focused on concrete properties after fire. It was found that concrete exposed to elevated temperatures experiences severe deterioration. However, research on hardened concrete after the occurrence of climatic changes seems to be very limited.

Retrofitted concrete can also be affected by high temperature, particularly the daily and seasonal temperature fluctuations. The bonding at the interface between concrete and repair materials is most likely to be affected. For improved resistance of concrete structures against penetration of harmful materials, good bonding is required at concrete interfaces. Due to the effect of temperature on the interface, interface failure can limit the performance of the repaired system. It is therefore necessary to study the performance of cement-based bi-materials after they have been subjected to thermal cycling.

2. Research significance

A bi-material is by definition the combination of two materials which are perfectly bonded. Application of any repair material results in a bi-material interface between the repair composite and the existing material of the retrofitted structure. The bonding at the interface is important for safety and durability. Failure of repaired system relates to cracking along the interface or kinking out of the interface. In the interface cracking case, the interface is relatively weaker than the bordering materials, so that the interface crack will propagate exclusively along the path of least resistance, i.e. the interface. In the crack kinking case, the interface is relatively stronger

* Corresponding author.
E-mail address: akan@ucy.ac.cy (A. Kanellopoulos).

0008-8846/$ – see front matter © 2009 Elsevier Ltd. All rights reserved.
doi:10.1016/j.cemconres.2009.07.008

than at least one of two adjoining materials. Quantitative evaluation of whether an interface crack will advance straight ahead or kink-out of the interface requires the knowledge of interfacial fracture toughness [10]. The research presented in this paper examines bi-material systems formed between a new class of ultra high-performance fibre-reinforced cementitious composite (UHPFRCC, denoted UHP hereinafter for brevity and for avoiding the use of its trade mark name CARDIFRC) and normal strength concrete (NSC) and high strength concrete (HSC).

3. Materials

UHP is a new class of ultra high-performance fibre-reinforced cementitious composite (UHPFRCC) characterized by high compressive strength, tensile/flexural strength and high energy absorption capacity. This has been made possible by incorporating steel fibres (6–13 mm long, 0.16 mm diameter) at high volume fractions (up to 8%) in a cementitious matrix densified by the use of silica fume. The matrix contains only very fine graded quartz sand, instead of ordinary river sand and coarse aggregates. By optimizing the grading of fine quartz sands, the water demand was considerably reduced without affecting the workability of the mix. This was achieved by adapting novel mixing procedures. Computer tomography imaging and sectioning of specimens confirmed that these techniques ensure remarkably homogeneous mix with a uniform distribution of fibres [11]. UHP consists of two different mix classes with similar properties. For the purpose of the current study only one of the mixes, called Mix I, is considered. The mix proportions and mechanical properties are given in Table 1.

The NSC and HSC mix designs, used in this study, were based on previous experimental work conducted in the same laboratory [12,13]. The mix proportions are presented in Table 2.

Both NSC and HSC specimens were cured for 28 days at 20 °C, whereas for UHP a hot curing procedure was followed as per the recommendation of the Patent (GB 2391010).

4. Experimental evaluation of fracture parameters of bi-materials

Tensile or shear bond strength is usually accepted as an interface property and it is in practice determined by a variety of test techniques [14]. However, both the tensile and shear bond strengths give essentially only a maximum value of the bond stress. It is very difficult to tell from the measurement technique if de-cohesion or separation is obtained in a brittle or ductile manner. Moreover, there is no information about the amount of energy needed for the separation of the materials. Therefore, the bond strength as such may be useful for ranking of repair materials, but it is not expected to have field performance predictive capability due to size and geometric effects. It is important to evaluate the bond properties after the maximum load in order to understand the failure process.

In fracture mechanics, the load–deformation curve contains all information that characterises fracturing of concrete. It is one of the fracture mechanics parameters and is suitable to evaluate the bond failure after the maximum load [15]. To obtain the load–deformation curve for a repaired structure, three-point bend or wedge splitting test (WST) can be used (Fig. 1). To date, there are only a few researchers who have used the WST for evaluating the performance of repaired system [16–20]. For the purposes of the research presented here, the WST has been adopted because of the compactness of specimens.

Table 1
Mix proportions and some material properties for CARDIFRC I.

Constituents	Mix I — (kg/m^3)
Cement — CEM-II 32.5R	855
Microsilica — undensified, 98.3% SiO_2	214
Quartz sand	
9–300 μm	470
250–600 μm	470
212–1000 μm	–
1–2 mm	–
Water	188
Superplasticiser–formaldehyde sulfonate	28
Fibres	
6 mm	390
13 mm	78
Water/cement	0.22
Water/binder	0.18
Material property	
Indirect tensile strength (MPa)	28.6
Compressive strength (MPa)	207.0
Size-independent specific fracture energy (J/m^2)	22,900

Table 2
Mix proportions for NSC and HSC.

	Cement	Fine aggregate	Coarse aggregate	Microsilica 98.3% SiO_2	Superplasticiser (%)	w/c
NSC	1	2	2.5	–	–	0.56
HSC	1	1.32	2.21	0.11	1.8	0.24

5. Experimental program

The test programme comprised of sixty-eight 200×200×200 (mm) cubes (Fig. 1b). Thirty six were monoliths (18 NSC and 18 HSC) and formed the control specimens. The remaining thirty-two were cast as bi-materials using UHP (Fig. 2a). In order to improve the bond between the repair material UHP and the parent concrete, the contacting surfaces of both materials were carefully cleaned of cement film and roughened to create secure mechanical interlocking between the adhesive and the concrete. This was achieved by creating a grid of shallow grooves with an angle grinder (Fig. 2b). The rough, irregular, and furrowed surface topography creates a structural morphology that allows the adhesive to penetrate into the irregularities, forming a strong interfacial layer. The bonding was done with a commercially available thixotropic epoxy adhesive. Once the adhesive hardened an artificial starter crack was created on the bonded specimen by notching along the interface with a diamond saw with a blade thickness of 3 mm. The mechanical and bonding properties of this adhesive which has been extensively used throughout the world are given in Table 3. Note that as one the objectives of this study was to check whether the bond could sustain thermal cycling without delamination, it was thought unnecessary to test the influence of thermal cycling on the bonding epoxy in isolation. In fact experience with the tests reported here and with a larger series of thermal cycling tests on reinforced concrete beams retrofitted with thin strips of UHP adhesively bonded with the same epoxy [21] conclusively proved that it is able to provide a secure bond without delamination.

Additionally to the above cube specimens, cubes (100 mm), cylinders (100×200 mm) and beams (100×100×500 mm) were cast from all types of concrete in order to obtain compressive strength,

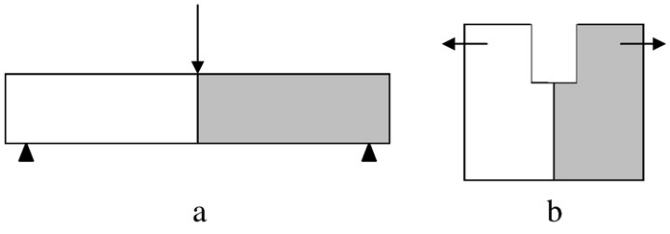

Fig. 1. Different composite geometry to determine the load–deformation curve for a bi-material.

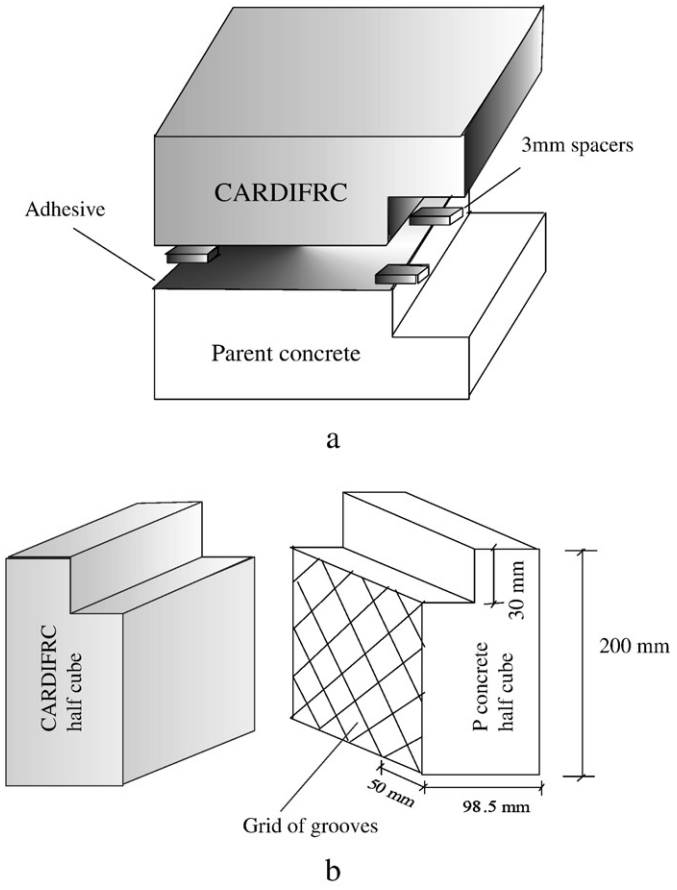

Fig. 2. Configurations of specimens and bonding techniques: (a) adhesive bonding procedure (b) roughened and grooved surface of concrete half cube.

indirect tensile strength, modulus of elasticity and modulus of rupture (MOR), respectively.

5.1. Thermal cycling

At the end of the respective curing regimes, all specimens were placed in an electrical furnace and heated to maximum temperature of 90 °C from a room temperature of 25 °C, in about 20 min. The aim was to keep the average heating rate at about 3°/min, to avoid the risk of the specimens being thermally shocked during heating. The maximum temperature was then maintained for another 8 h before the beams were cooled down to the room temperature in a further 16 h. The above 24-hour heating, hold and cooling period constitutes one thermal cycle which mimics the temperature fluctuations in hot arid climate when the exposed surfaces of concrete are known to reach very high temperatures during the daytime. The specimens were exposed to 30 and 90 thermal cycles. After the requisite number of thermal cycles, the specimens were tested at room temperature.

Table 3
Technical and physical data of the epoxy based adhesive used in the study.

Secant flexural modulus of elasticity (BS 6319) at 7 days	5.8 GPa
Compressive strength (BS 6319) at 24 h	35 MPa
Compressive strength (BS 6319) at 7 days	55 MPa
Flexural strength (BS 6319) at 7 days	22 MPa
Tensile strength (BS 6319) at 7 days	6 MPa
Adhesion to concrete	3.5 MPa

5.2. Experimental evaluation of fracture properties

For determining the fracture properties, the cube specimens were notched with notch to depth ratios of 0.20 and 0.50. The specimens were notched before the commencement of thermal cycling. Following the notching and thermal cycling, two steel load transmission pieces fitted with roller bearings were placed on either side of specimens. A steel wedge was placed between the roller bearings (Fig. 3a). A vertical force on the wedge imparts a well-defined horizontal-force to the bearings thus wedging open the starter crack. The rate of loading was controlled by a crack mouth opening displacement (CMOD) gauge at a very low rate (0.0002 mm/s) so that the fracture occurred in a stable manner. During the propagation of the crack in the specimens, the deformation is measured by the crack mouth opening displacement (CMOD) (Fig. 3b).

The area under the load–CMOD curve corresponds to the work required to separate the specimens. Dividing this work of fracture by the ligament area that was intact before the test began yields the measured specific fracture energy G_f which depends on the notch to depth ratio

$$G_f = \frac{1}{(W^* - a)B}\int F_H d(\mathrm{CMOD}) \tag{1}$$

where B is the specimen thickness and $W^* = W - d_n$ (see Fig. 4).

However, from the measured G_f it is important to evaluate the size-independent specific fracture energy. Based on the boundary effect model of Duan et al. [22] for determining the size-independent fracture energy, Abdalla and Karihaloo [23] found that the size-independent fracture energy can be determined by testing just two specimens of the same size one containing a shallow and the second a deep starter notch [23]. This was the reason that tests presented here were conducted on wedge type specimens with two notch to depth ratios $a/W = \alpha = 0.20$ and $\alpha = 0.50$. The determination of the size-independent specific fracture energy G_F for concrete was based on the following equation:

$$G_f(a/W) = \begin{cases} G_F\left[1 - \frac{1}{2}\cdot\frac{a_1/W}{1 - a/W}\right] & 1 - a/W > a_1/W \\ G_F\cdot\frac{1}{2}\cdot\frac{(1 - a/W)}{a_1/W} & 1 - a/W \le a_1/W \end{cases}. \tag{2}$$

The final step in the calculation of fracture parameters with which we are concerned in this paper is the brittleness. Brittleness of a mix is defined as the tendency of the mix to fracture abruptly before significant irreversible deformation occurs. Hillerborg et al. [24] proposed the characteristic length l_{ch} as a measure of brittleness for concrete:

$$l_{ch} = \frac{G_F E_c}{f_t^2} \tag{3}$$

where f_t is the tensile strength of the concrete, G_F is the size-independent specific fracture energy and E_c the modulus of elasticity. Since l_{ch} includes a combination of toughness, stiffness and strength parameters of a concrete mix, the larger the value of l_{ch} the less brittle the concrete mix.

6. Characterisation of cracks at bi-material interfaces

The characterisation of cracks at bi-material interfaces substantially differs from that in homogenous materials. Unlike homogeneous materials, bi-material exhibits a coupling of tensile and shear effects. The stress field is characterized by a complex stress intensity factor, K, together with the bi-material constant ε related to the elastic properties of the two materials. An alternative characterization of the near-tip stress field involves the energy release rate G, together with the mode mixity χ. The mode mixity is a quantity measuring the

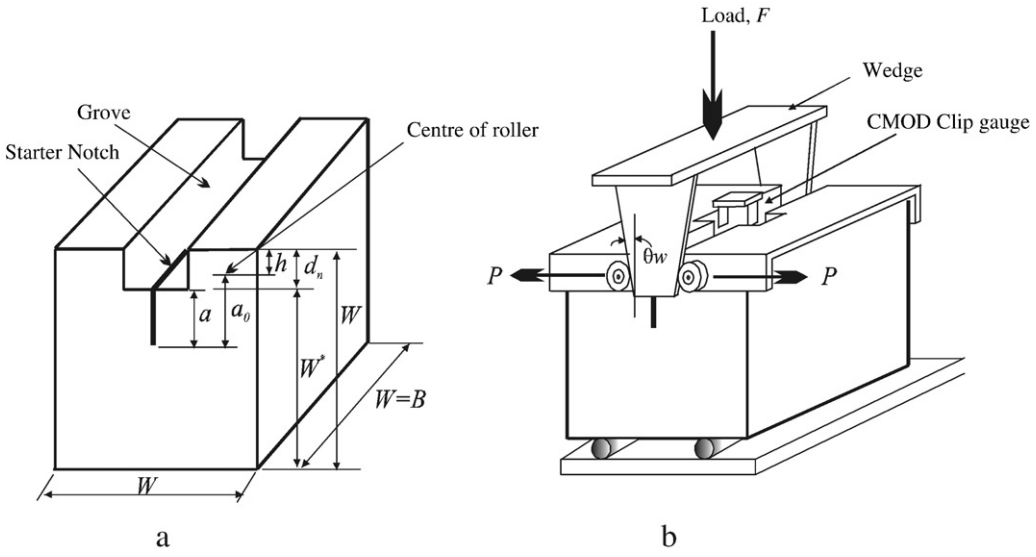

Fig. 3. Configuration of WS test: (a) specimen shape, (b) loading arrangement.

ratio between the shear and normal stresses at the interface in front of the crack-tip.

Assume two isotropic elastic solids joined along the x-axis (Fig. 5). Let E_j, and n_j denote the Young modulus and the Poisson ratio of the j-th material ($j=1, 2$), respectively. The corresponding shear modulus is obtained through:

$$\mu_j = \frac{E_j}{2\left(1+\nu_j\right)}. \tag{4}$$

When a crack lies along the bi-material interface of two dissimilar isotropic elastic media, the near-tip stress field is an oscillatory singular field, which can be written [25–28] as:

$$\sigma_{ij} = \mathrm{Re}\left\{\frac{Kr^{i\varepsilon}}{\sqrt{2\pi r}}\right\}\tilde{\sigma}_{ij}^{I}(\theta,\varepsilon) + \mathrm{Im}\left\{\frac{Kr^{i\varepsilon}}{\sqrt{2\pi r}}\right\}\tilde{\sigma}_{ij}^{II}(\theta,\varepsilon). \tag{5}$$

Here r and θ are the polar coordinates; Re and Im denote real and imaginary parts; K is the complex stress intensity factor; $\tilde{\sigma}_{ij}^{I}$ and $\tilde{\sigma}_{ij}^{II}$ are the dimensionless angular functions of θ and ε [28], and the bi-material constant ε is defined by:

$$\varepsilon = \frac{1}{2\pi}\ln\left(\frac{k_1/\mu_1 + 1/\mu_2}{k_2/\mu_2 + 1/\mu_1}\right) \tag{6}$$

where k_j and μ_j are Lamé constants and subscripts 1 and 2 refer to the materials 1 and 2, respectively. The quantity α vanishes when the two materials are identical. The solution of elastic plane problems for bi-material depends only on two non-dimensional combinations of the elastic moduli, called Dundurs' parameters α and β. Physically, α measures the magnitude of mismatch of the elastic tensile moduli of the two bi-materials and β measures the mismatch in their plane bulk moduli:

$$\alpha = \frac{\mu_1(k_2+1) - \mu_2(k_1+1)}{\mu_1(k_2+1) + \mu_2(k_1+1)} \tag{7}$$

$$\beta = \frac{\mu_1(k_2-1) - \mu_2(k_1-1)}{\mu_1(k_2+1) + \mu_2(k_1+1)}. \tag{8}$$

Therefore, the parameter ε can be rewritten as:

$$\varepsilon = \frac{1}{2\pi}\ln\left(\frac{1-\beta}{1+\beta}\right). \tag{9}$$

The energy release rate G is related to K by:

$$G = \frac{\left(1-\beta^2\right)}{E_*}\left(K_I^2 + K_{II}^2\right) = \frac{\left(1-\beta^2\right)}{E_*}|K|^2 \tag{10}$$

where $|K|$ is the modulus of K and the effective $E_* = 2E_1'E_2'/(E_1'+E_2')$, in which $E' = E/(1-\nu^2)$ for plane strain problems and $E' = E$ for plane stress problems and ν is the Poisson ratio. Using the asymptotic field Eq. (5), the tractions at a distance r ahead of the crack-tip along

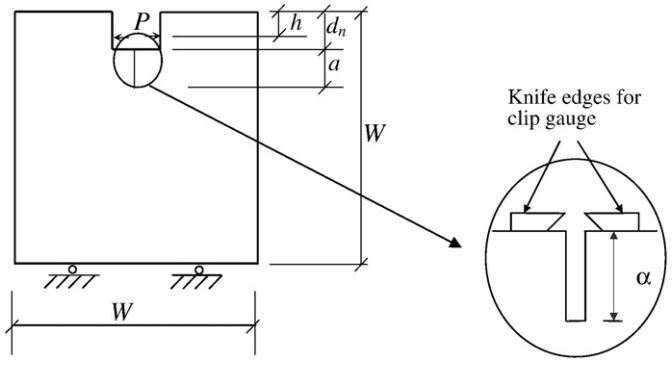

Fig. 4. The points of application of wedge force and the location of clip gauge for measuring CMOD.

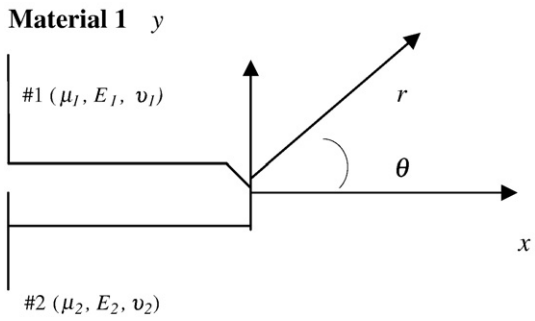

Fig. 5. Geometry of a bi-material system with an interface crack.

the interface ($\theta = 0$) can be expressed according to Hutchinson et al. [29] as:

$$(\sigma_{22} + i\sigma_{12})_{\theta=0} = \frac{Kr^{i\varepsilon}}{(2\pi)^{1/2}}. \quad (11)$$

According to dimensional analysis [30], the modulus of $|K|$ has the dimension

$$|K| = [\text{stress}][\text{length}]^{(1/2)-i\varepsilon}. \quad (12)$$

Obviously, the dimension of the modulus $|K|$ is quite different from that of homogeneous materials.

7. Results and discussion

7.1. Mechanical properties

The compressive strength, tensile strength, elasticity modulus and MOR results for all types of concrete after 0, 30 and 90 thermal cycles are shown in Table 4. The results reveal a relative increase in the compressive strength f_c at elevated temperature of 90 °C, irrespective of the number of thermal cycles and type of material. The increase in compressive strength can be attributed to on-going hydration [31,32] which is accelerated at elevated temperatures. For HSC and UHP the phenomenon is most likely due to the presence of microsilica that activates the secondary reaction and leads to an additional strength. For NSC, it may also be due to the fact that water, bound by capillary condensation, is partially expelled [33] and thus available for further hydration. In the case of indirect tensile strength it is quite clear that the elevated temperatures assist the on-going hydration which leads to a gain in strength at low cycles. However, the reduction in strength (for NSC and HSC) at 90 thermal cycles could be due to the weakening of the surface forces (van der Waals forces) between the gel particles, or due to the stresses generated at the interface between the aggregate and hardened cement paste. These stresses induce damage through micro-cracks. The results also show that the splitting strength of UHP follows a monotonically increasing trend.

The same trend, as for the indirect tensile strength, is also observed in the flexural strength values (MOR). For both NSC and HSC an increase is observed at low cycles and a small decrease at 90 cycles, whereas UHP exhibits a slight increase in flexural strength at all stages of thermal treatment. The same is noticed in the modulus of elasticity. This observation is in agreement to the findings of Schneider [34]. The decrease in stiffness after 90 thermal cycles is most likely due to the internal micro-cracks caused by thermal cycling, especially at the interface between cement paste and coarse aggregates. Unfortunately, no samples were taken from the bulk to confirm this reasonable hypothesis. The tests showed that the modulus of elasticity for UHP is not affected by thermal cycling, possibly because of the stronger interface between the densified paste and hard phases.

Table 4
The mechanical properties of NSC, HSC and UHP after thermal cycling.

TC		f_{cu} (MPa)	f_t (MPa)	MOR (MPa)	E (GPa)
0	NSC	41.60 (2.6)	3.80 (7.3)	5.44 (1.2)	32.00
	HSC	102.30 (1.2)	7.72 (1.7)	9.72 (2.2)	47.40
	UHP	199.93 (0.3)	27.00 (2.7)	32.80(4.0)	48.00
30	NSC	46.33 (3.8)	4.10 (1.9)	6.43 (2.8)	35.21
	HSC	131.06 (2.5)	7.93 (3.7)	10.61 (2.3)	48.70
	UHP	224.30 (1.3)	30.71 (5.4)	33.47 (6.3)	49.00
90	NSC	45.80 (0.7)	3.85 (2.5)	5.78 (1.5)	28.00
	HSC	131.60 (2.5)	7.59 (1.2)	9.96 (4.7)	42.00
	UHP	225.03 (1.8)	31.02 (6.2)	33.73 (9.2)	49.00

Note: TC = Thermal Cycles; figures in parentheses give coefficient of variation (%).

7.2. Fracture tests

The measured fracture properties of the control as well as of the bonded specimens are presented in Table 5. As expected, the G_f decreases in all specimens as the notch to depth ratio increases. This is primarily due to the fact that the propagating crack encounters resistance from more coarse aggregate particles for shorter initial notches. Second, the probability of flaws like voids, micro-cracks and bond cracks in the path of the growing crack increases with increasing ligament length [1,35].

Fig. 6 illustrates the response of control NSC and UHP–NSC specimens. As expected, since the crack in both the control and bonded specimens propagated in the normal strength concrete, the fracture mode is classified as quasi-brittle for zero thermal cycles (Fig. 7). It can be seen that the stiffness and maximum failure load for bonded specimens increase compared to the control ones. These results indicate that the bonded specimens offer somewhat greater resistance to the crack growth than the control specimens (Table 5). The Load–CMOD curves shown in Fig. 6a and d reveal that bonding NSC to UHP improves the peak load, reduces the pre-peak non-linearity, and the post-peak behaviour is steeper. The latter indicates that there is a slight decrease in G_f value for bonded specimens compared to that of control NSC. The reduction in fracture energy for bonded NSC could also be attributed to the fact that the crack path in such a bonded system is less tortuous than that in the control NSC specimens. This reduction is quite noticeable in specimens with a notch to depth ratio of 0.50 (Fig. 6d).

The same response is observed after 30 cycles of heat treatment (Fig. 6b and e). However, the post-peak response of bonded specimens seems to be steeper, which indicates that the bonded specimens are slightly more brittle than the control specimens. As can be seen, the stiffness and maximum load of bonded specimens are higher than those of control specimens. The load–CMOD response of the specimens does not change even after 90 cycles (Fig. 6c and f). Nonetheless, the increase in maximum load between the control and bonded specimens seems less than before.

Table 5
The measured fracture parameters for all specimen configurations.

TC/type of specimen	α	G_f (N/m)	G_F (N/m)	α_l (mm)	l_{ch} (mm)
0					
NSC	0.20	115.76 (5.6)			
	0.50	95.58 (2.3)	148.00	36.00	327.97
HSC	0.20	83.63 (5.9)			
	0.50	51.70 (1.7)	136	62.20	108.16
UHP–NSC	0.20	107.43 (7.6)			
	0.50	82.35 (6.6)	149.24	44.80	
UHP–HSC	0.25	80.33 (5.0)			
	0.55	52.23 (4.6)	122	31.60	
30					
NSC	0.20	121.52 (6.8)			
	0.50	100.73 (0.1)	158.00	43.00	330.94
HSC	0.20	86.42 (5.4)			
	0.50	54.49 (5.2)	140.00	61.22	108.42
UHP–NSC	0.20	122.00 (3.5)			
	0.50	98.00 (10.7)	162.00	40.00	
UHP–HSC	0.25	86.12 (2.5)			
	0.55	54.80 (3.7)	134.00	53.70	
90					
NSC	0.20	108.00 (8.1)			
	0.50	88.63 (5.9)	141.00	37.00	268.73
HSC	0.20	82.04 (8.9)			
	0.50	57.19 (3.9)	123.00	53.90	89.67
UHP–NSC	0.20	107.33 (1.9)			
	0.50	80.90 (3.5)	151.38	46.60	
UHP–HSC	0.25	73.22 (8.5)			
	0.55	55.38 (2.1)	100.50	40.74	

Note: TC = Thermal Cycles; figures in parentheses give coefficient of variation (%).

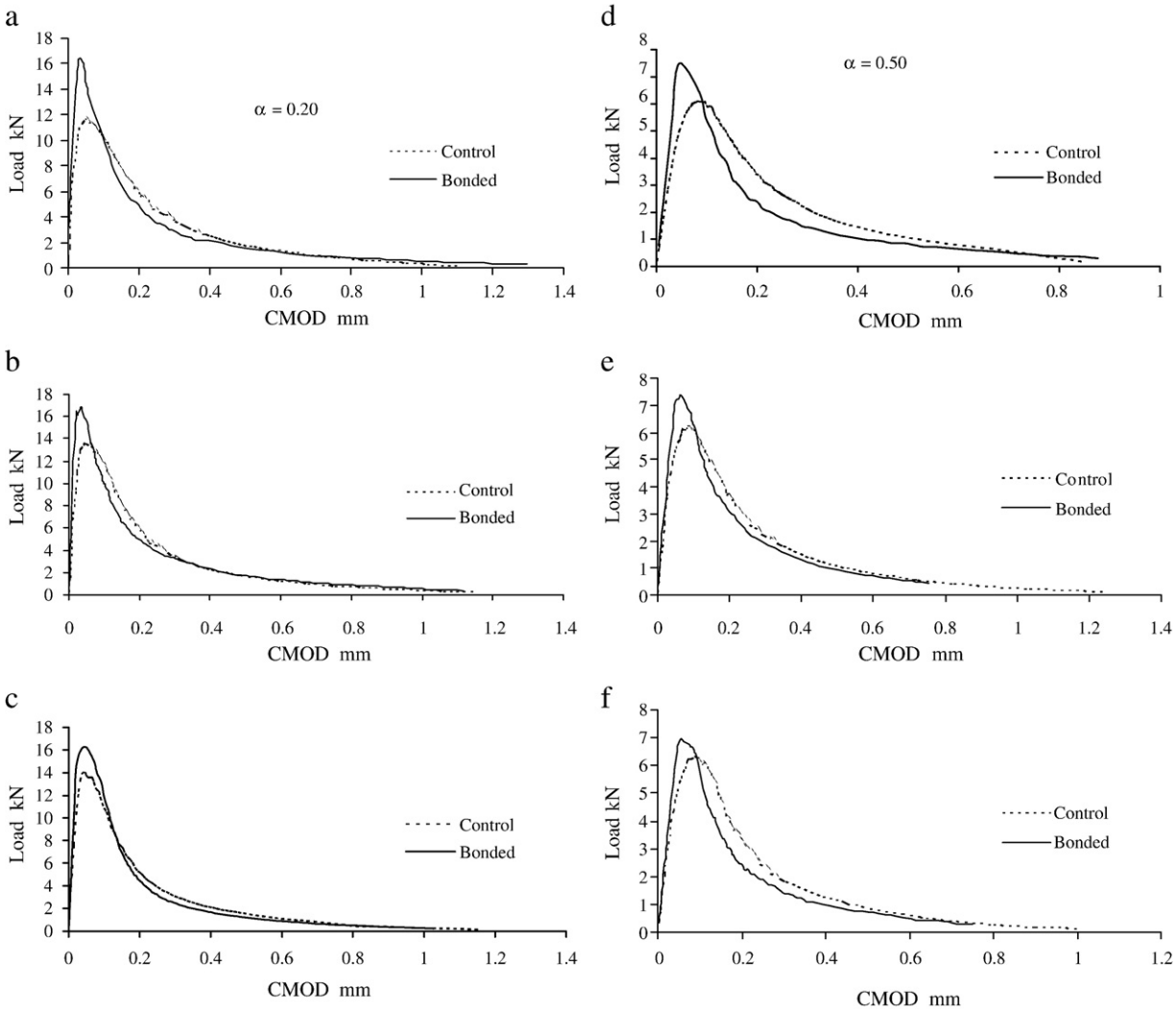

Fig. 6. Load–CMOD curves for control and bonded NSC specimens with $\alpha = 0.20$, after: (a) zero thermal cycles, (b) 30 thermal cycles, (c) 90 thermal cycles, and with $\alpha = 0.50$ after (d) zero thermal cycles, (e) 30 thermal cycles and (f) 90 thermal cycles, respectively.

As can be observed from Table 5, in the case of HSC and UHP bonded specimens the notch to depth ratios used are different (0.25 and 0.55) than those used for NSC above (0.20 and 0.50). The reason is that in an initial trial test a diagonal shear failure was observed at the corner of the groove (Fig. 8a). This was because the strength there had been exceeded before the starter notch could propagate, indicating

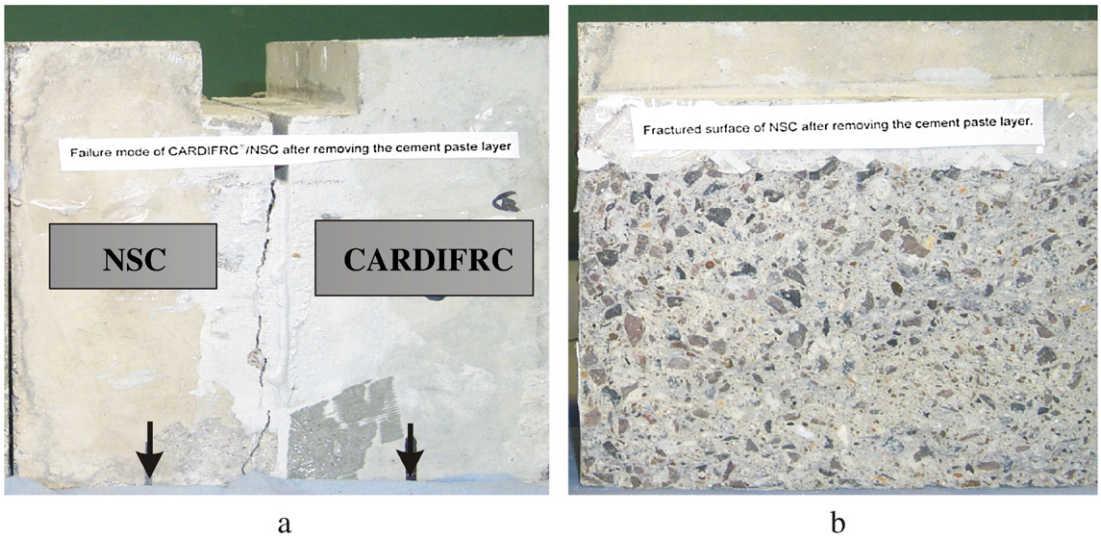

Fig. 7. The NSC–UHP system after failure: (a) the diagonal failure crack through the weakest material, (b) the failure interface.

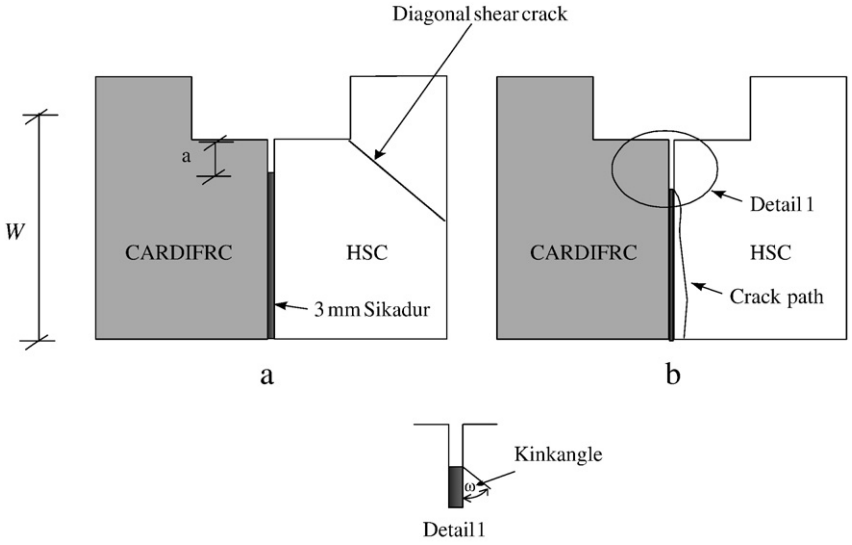

Fig. 8. Schematic representation for tested UHP/HSC: (a) α(0.20) with diagonal shear failure, (b) α(0.25) crack propagation through the HSC.

insufficient starter notch depth. Therefore, the notch to depth ratio α was increased from 0.20 to 0.25. As expected, after increasing α from 0.20 to 0.25 a crack started at the corner of the initial notch and propagated into the concrete (Fig. 8b). Also, for the HSC specimens a deeper initial notch $\alpha = 0.55$ has been used (instead of $\alpha = 0.50$ as in control HSC) to maintain the necessary spread between the starter notch depths [23].

In the HSC–UHP bonded specimens, a crack started at a corner of the starter notch and always kinked into the parent concrete at an angle of about 10° for specimens with a notch to depth ratio of 0.25 and about 8° for specimens with a notch to depth ratio of 0.55. After the thermal treatment the failure mechanism for all specimens is similar to those of bonded NSC–UHP. In all specimens, as in the case of zero thermal cycles, the crack formed at the corner of starter notch and kinked towards the parent concrete at an angle of about 10° and 8° for specimens with notch to depth ratios of 0.25 and 0.55, respectively. The crack then propagated in the concrete adjacent to the interface. Fig. 9 shows the comparison between the specific size-independent fracture energy for both control and bi-material systems.

As can be seen, the G_F for bonded specimens is less than that of control specimens after 0 and 30 thermal cycles. This indicates that the bonded system is slightly more brittle. Although there was no deterioration visible to the naked eye because of thermal cycling, the decrease in fracture energy after 90 thermal cycles could be associated with internal micro-cracking in HSC.

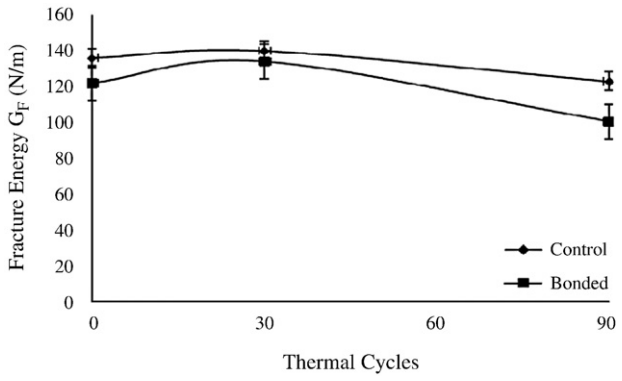

Fig. 9. The effect of thermal cycling on the size-independent fracture energy of control and HSC–UHP bonded specimens.

Based on the linear elastic fracture mechanics (LEFM) analysis of bi-material systems, the following analytical expressions will provide a plausible qualitative explanation for the observed increase in the maximum failure load of bonded specimens over that of control specimens [36]. Assuming the Poisson ratios of the two materials are the same, the Dundurs' elastic mismatch parameter is

$$\alpha = \frac{E_1 - E_2}{E_1 + E_2} \tag{13}$$

and the second Dundurs' parameter β is ≈ 0. This simplifies the estimation of fracture energy.

Substituting β in Eq. (10) gives:

$$G_{com} = \frac{1}{E_*} K_*^2 \tag{14}$$

where G_{com} is the energy release rate for the composite system, K_* and E_* are the effective stress intensity factor and effective modulus of elasticity respectively. The latter is connected with the moduli of elasticity of the two materials with Eq. (15).

$$\frac{1}{E_*} = \frac{1}{2}\left(\frac{1}{E_1} + \frac{1}{E_2}\right) \tag{15}$$

Since $E_* = E_{com}$ and E_1 and E_2 are equal to E_{NSC} and $E_{CARDIFRC}$

$$G_{com} = \frac{1}{2}\left(\frac{1}{E_{NSC}} + \frac{1}{E_{CARDIFRC}}\right) K_*^2 \tag{16}$$

Thus

$$K_* = \sqrt{\frac{2G_{com}}{\frac{1}{E_{NSC}} + \frac{1}{E_{CARDIFRC}}}} = \sqrt{\frac{2G_{com}E_{NSC}E_{CARDIFRC}}{(E_{CARDIFRC} + E_{NSC})}} \tag{17}$$

Since G_F of NSC is roughly equal to G_{com} and K_I of NSC is equal to $\sqrt{E_{NSC}G_F}$, at the same level of applied K_I, the ratio

$$\sqrt{\frac{2E_{CARDIFRC}}{E_{CARDIFRC} + E_{NSC}}} > \sqrt{\frac{100}{84}} = 1.09 \tag{18}$$

As a result, it follows from Eq. (17) that $K_* > K_I$

This means that the maximum load level corresponding to the initiation of crack growth must be larger in the bonded system (P_{*max}) than the solid NSC (P_{max}) which is what has been observed in tests. Note that the initiation of crack growth even in bi-material systems is governed by mode I loading, whereas the direction of kinking is governed by mode II loading and the Dundurs parameters [37].

8. Conclusions

In the light of what has been discussed regarding the fracture behaviour of the individual materials and of the interface between cement-based bi-materials, the following conclusions can be drawn:

- The mechanical and fracture properties of NSC and HSC are substantially improved after 30 thermal cycles, but less so after 90 thermal cycles. The increase in these properties after 30 thermal cycles is probably due to the continued hydration of unhydrated cement. However, the reduction after 90 thermal cycles could be due to the initiation of micro-cracks between the paste and hard phases.
- The mechanical properties of the UHP are improved even after 90 thermal cycles. This could be attributed to the continued hydration of unhydrated cement and to the presence of microsilica that activates the secondary reaction. The presence of fibres seems to counteract any possible deterioration due to micro-cracking.
- NSC and HSC can be successfully repaired with the UHP using the technique of adhesive bonding.
- To prevent delamination or interfacial fracture, both the UHP and the parent concrete mating surfaces have to be thoroughly cleaned of any residual cement film and roughened. i.e., when the surfaces of both concrete and UHP are deliberately roughened, a better rough surface of the substrate is created and this leads to higher interface toughness which delays interface crack propagation forcing the crack to kink into the weaker material and to eventually propagate through the concrete.
- The load carrying capacity of bonded concrete appears to be higher than that of control specimens and moreover the failure mode of bonded system remained almost unchanged even after thermal cycling.
- No visual deterioration or bond degradation was observed after thermal cycling of the bonded specimens attesting to the good thermal compatibility between the concrete and UHP.
- The measured fracture energy $G_f(\alpha)$ of bonded specimens decreases with increasing notch to depth ratios. The $G_f(\alpha)$ and the size-independent specific fracture energy G_F for control and bonded specimens varies with thermal cycling due to the observed change in the mechanical properties of concrete.

References

[1] B.L. Karihaloo, Fracture Mechanics and Structural Concrete, Addison Wesley Longman, London, 1995.
[2] C. Castillo, A.J. Durrani, Effect of transient high temperature on high-strength concrete, ACI Mater. J. 87 (1) (1990) 47–53.
[3] V.V. Bertero, M. Polivka, Influence of thermal exposures on mechanical characteristics of concrete, ACI Special Publication 1(34), International Seminar on Concrete for Nuclear Reactors, ACI, Detroit, 1972, pp. 505–531.
[4] C. Berwanger, X. Sarkar, Effect of Temperature and Age on Thermal Expansion and Modulus of Elasticity of Concrete, Behaviour of Concrete under Temperature Extremes, SP-39, American Concrete Institute, Farmington Hills, 1973, pp. 1–22.
[5] N.K. Bairagi, N.S. Dubal, Effect of thermal cycles on the compressive strength, modulus of rupture and dynamic modulus of concrete, Indian Concr. J. (1996) 423–426.
[6] H. Abdel-Fattah, S. Hamoush, Variation of the fracture toughness of concrete with temperature, Constr. Build. Mater. 11 (2) (1997) 105–108.
[7] Z.P Bazant, P.C. Prat, Effect of temperature and humidity on fracture energy of concrete, ACI Mater. J. 85 (1988) 262–271.
[8] G. Baker, The effect of exposure to elevated temperatures on the fracture energy of plain concrete, Mater. Struct. 29 (1996) 383–388.
[9] Z. Zhang, N. Bicanic, C. Pearce, G. Balabanic, Residual fracture properties of normal and high strength concrete subjected to elevated temperatures, Mag. Concr. Res. 52 (2) (2000) 123–136.
[10] V.C. Li, Y.M. Lim, D.J. Foremsky, Interfacial fracture toughness of concrete repair materials, in: F.H. Wittman (Ed.), Proceedings of Fracture Mechanics of Concrete Structures II, AEDIFICATIO Publishers, 1995, pp. 1329–1344.
[11] S.D.P. Benson, D. Nicolaides, B.L. Karihaloo, CARDIFRC — development and mechanical properties. Part II: fibre distribution, Mag. Concr. Res. 57 (8) (2005) 412–432.
[12] M.R. Taylor, F.D. Lydon, B.I. Barr, Mix proportions of high strength concrete, Constr. Build. Mater. 10 (6) (1996) 445–450.
[13] H.F. Abousaif, Damage and fracture behaviour of concrete, PhD Thesis, Cardiff University, Cardiff School of Engineering, 1997.
[14] P.H. Emmons, Concrete Repair and Maintenance Illustrated, Concrete Publishers and Consultants, Kingston, England, 1994.
[15] M. Kunieda, N. Kurihara, Y. Uchida, K. Rokugo, Application of tension softening diagrams to evaluation of bond properties at concrete interfaces, Eng. Fract. Mech. 65 (2000) 299–315.
[16] E.K. Tschegg, S.E. Stanzel, Adhesive power measurements of bonds between old and new concrete, J. Mater. Sci. 26 (1991) 5189–5194.
[17] E.K. Tschegg, H.M. Rotter, P.E. Roelfstra, U. Bourgund, P. Jussel, Fracture mechanical behaviour of aggregate–cement matrix interfaces, J. Mater. Civ. Eng. (1995) 199–203.
[18] E.K. Tschegg, An efficient fracture test method for bituminous and layer bonds. Mechanical tests for bituminous material, in: H. Di Benedetto, L. Francken (Eds.), Proceedings of the Fifth International RILEM Symposium, RILEM Paris, 1997, pp. 405–411.
[19] A.M. Irhouma, M.L. Ayari, L.C. Robinson, Effect of low temperature on fracture energy of concrete joints and repair materials, in: H. Mihashi, K. Rokugo (Eds.), Fracture Mechanics of Concrete Structures, vol. III, AEDIFICATIO Publishers, Freiburg, Germany, 1998, pp. 1593–1604.
[20] H. Harmuth, Investigation of the adherence and the fracture behaviour of polymer cement concrete, Cem. Concr. Res. 25 (3) (1995) 497–502.
[21] F.A. Farhat, D. Nicolaides, A. Kanellopoulos, B.L. Karihaloo, CARDIFRC — performance and application to retrofitting, Eng. Fract. Mech. 74 (1–2) (2007) 151–167.
[22] K. Duan, X.Z. Hu, F.H. Wittmann, Boundary effect on concrete fracture induced by non-constant fracture energy distribution, in: R. De Borst, J. Mazars, G. Pijaudier-Cabot, J.G.M. Van Mier (Eds.), Fracture Mechanics of Concrete Structures (Proc. FRAMCOS-4), A.A. Balkema Publishers, The Netherlands, 2001, pp. 49–55.
[23] H.M. Abdalla, B.L. Karihaloo, Determination of size-independent specific fracture energy of concrete from three-point bend and wedge splitting tests, Mag. Concr. Res. 55 (2) (2003) 133–141.
[24] A. Hillerborg, M. Modéer, P.E. Petersson, Analysis of crack formation and crack growth in concrete by means of fracture mechanics and finite elements, Cem. Concr. Res. 6 (1976) 773–782.
[25] M.L. Williams, The stress around a fault or crack in dissimilar media, Bull. Seismol. Soc. Am. 49 (1959) 199–204.
[26] J.R. Rice, G.C. Sih, Plane problems of cracks in dissimilar media, J. Appl. Mech. (1965) 418–423.
[27] H. England, A crack between dissimilar media, J. Appl. Mech. 32 (1965) 400–402.
[28] C.F. Shih, R. Asaro, Elastic–plastic analysis of cracks on bimaterial interfaces; part 1: small scale yielding, J. Appl. Mech. 55 (1988) 299–316.
[29] J.W. Hutchinson, M.E. Mear, J.R. Rice, Crack paralleling an interface between dissimilar materials, J. Appl. Mech. 54 (1987) 828–832.
[30] J.R. Rice, Elastic fracture mechanics concepts for interfacial cracks, J. Appl. Mech. Trans. ASME 55 (1998) 98–103.
[31] A.M. Neville, Properties of Concrete, 4th Ed., Longman Group, UK and New York: John Wiley & Sons, 1995.
[32] Z. Zhang, N. Bicanic, C. Pearce, D. Phillips, Relationship between brittleness and moisture loss of concrete exposed to high temperatures, Cem. Concr. Res. 32 (2002) 363–371.
[33] F.S. Rostasy, H. Budelmann, Strength and deformation of concrete with variable content of moisture at elevated temperature up to 90 °C, Cem. Concr. Res. 16 (1986) 353–362.
[34] U. Schneider, Concrete at high temperatures — a general review, Fire Saf. J. 13 (1988) 55–68.
[35] P. Nallathambi, A study of fracture of plain concrete, PhD Thesis, University of Newcastle, N.S.W, Australia, 1986.
[36] F.A. Farhat., Performance of concrete structures retrofitted with CARDIFRC® after thermal cycling, PhD Thesis, Cardiff University, Cardiff School of Engineering, 2004.
[37] B.L. Karihaloo, Crack kinking and curving, Mech. Mater. 1 (1982) 189–201.